MOLECULAR AND CELLULAR BIOLOGY, July 2005, p. 6289–6302 Vol. 25, No. 14
0270-7306/05/$08.00+0 doi:10.1128/MCB.25.14.6289–6302.2005

Impaired Mitotic Progression and Preimplantation Lethality in Mice Lacking OMCG1, a New Evolutionarily Conserved Nuclear Protein†

Jérôme Artus,[1] Sandrine Vandormael-Pournin,[1] Morten Frödin,[1]‡ Karim Nacerddine,[2] Charles Babinet,[1] and Michel Cohen-Tannoudji[1]*

Unité de Biologie du Développement, CNRS URA 2578,[1] and Unité d'Organisation Nucléaire et Oncogénèse, INSERM U 579,[2] Institut Pasteur, 25 rue du Dr Roux, 75724 Paris Cedex 15, France

Received 15 December 2004/Returned for modification 19 January 2005/Accepted 4 April 2005

While highly conserved through evolution, the cell cycle has been extensively modified to adapt to new developmental programs. Recently, analyses of mouse mutants revealed that several important cell cycle regulators are either dispensable for development or have a tissue- or cell-type-specific function, indicating that many aspects of cell cycle regulation during mammalian embryo development remain to be elucidated. Here, we report on the characterization of a new gene, *Omcg1*, which codes for a nuclear zinc finger protein. Embryos lacking *Omcg1* die by the end of preimplantation development. In vitro cultured *Omcg1*-null blastocysts exhibit a dramatic reduction in the total cell number, a high mitotic index, and the presence of abnormal mitotic figures. Importantly, we found that *Omcg1* disruption results in the lengthening of M phase rather than in a mitotic block. We show that the mitotic delay in *Omcg1*$^{-/-}$ embryos is associated with neither a dysfunction of the spindle checkpoint nor abnormal global histone modifications. Taken together, these results suggest that *Omcg1* is an important regulator of the cell cycle in the preimplantation embryo.

The cell cycle is a collection of highly ordered processes that results in the duplication of a cell and the faithful transmission of the genetic information to two daughter cells. Many essential developmental processes including proliferation, growth, patterning, and differentiation require the cell cycle to be closely coordinated with various signaling pathways. As a consequence, and despite a largely conserved basic organization among eukaryotes, the progress of cells through all phases of the cell cycle may be extensively modified during development in order to meet the demands of a given cell at specific stages. Hence, the G_1 phase, the main period of cell growth, is the target of many regulatory pathways and appears extremely variable in length (39). How plastic the normal cell cycle is becomes clear when comparing the so-called "embryonic cleavage cycles" and the endoreplication cycle, also referred to as the endocycle. The former, which take place in most metazoans except mammals, follow fertilization and can be extremely fast (less than 10 min in *Drosophila* embryo) (7, 35); furthermore, they lack the G_1 and G_2 gap phases and certain checkpoint controls, which ensure that a given step is properly achieved before growth progresses to the next step of the cycle (8). The embryonic cleavage cycles are maternally driven as nutrients and cell cycle factors are stored in the egg cytoplasm during oogenesis. On the other hand, in endocycles, DNA replication (the S phase) and cell growth take place without an intervening mitosis (M phase) phase leading to polyploidy. The endocycle is widespread among multicellular organisms and is associated with growth and differentiation (e.g., nurse cells and follicular cells of the *Drosophila* oocyte cyst).

Several transitions in the organization of the cell cycle are observed during early mammalian development. As in other multicellular organisms including vertebrates, mammalian development also begins by a process called cleavage consisting of a series of mitotic divisions with no increase in embryo size. However, and in striking contrast to other species, the mammalian zygote divides slowly. In the mouse, the first mitotic division, which is maternally driven, occurs 16 to 18 h after fertilization. At the two-cell stage, transcription of the zygotic genome occurs and is required for the following cleavages to happen (11). The next four cell cycles average 12 h each, leading to the 32-cell early blastocyst (16). Furthermore, these cycles have a G_1 and a G_2 phase and are endowed with DNA damage and spindle checkpoints (see, for example, references 13, 18, and 46). The blastocyst contains two cell types: the trophectoderm (TE) that gives rise to the placenta and an inner cell mass (ICM) from which the whole fetus and part of the extraembryonic tissues will develop. After implantation, differentiation of trophoblast giant cells, which are involved in the remodeling of the maternal uterus during implantation, is achieved through several endocycles leading to increases of DNA content up to 1000N (48). In the embryo proper, areas within the embryonic ectoderm have a cell cycle time of approximately 3 h (31, 45). These rapid cell cycles of the early postimplantation rodent embryo share many features with those of the rapid cleavage cycles of early frog or drosophila embryos such as short or nonexistent G_1 and G_2 phases and lack of checkpoint control in response to DNA damage (reviewed in reference 36).

While the cell cycle machinery has been highly conserved through evolution, it is now clear that the cell cycle has been modified in diverse and novel ways to adapt to new develop-

* Corresponding author. Mailing address: Unité de Biologie du Développement, CNRS URA 2578, Institut Pasteur, 25 rue du Dr Roux, 75724 Paris Cedex 15, France. Phone: 33 1 45 68 84 86. Fax: 33 1 45 68 86 34. E-mail: m-cohen@pasteur.fr.

† Supplemental material for this article may be found at http://mcb.asm.org/.

‡ Present address: The Kinase Signalling Laboratory, Biotech Research and Innovation Centre, Fruebjergvej 3, 2100 Copenhagen, Denmark.

mental programs elaborated during evolution (26). The canonical view about the control of the cell cycle is actually being challenged by in vivo studies. Thus, until recently it was accepted that several Cdk/cyclin complexes were essential for the control of the successive steps of the cell cycle. Surprisingly, however, mice lacking either cyclin E1 and cyclin E2 or Cdk2, all assumed to be essential to initiate the S phase, were found to be viable (2, 14, 37, 40). Similarly, most tissues can develop normally in the absence of cyclin D1/D2/D3-Cdk4/6 complexes (21, 33). These observations could be extended to other cell cycle regulators (reference 2 and references therein). Thus, it appears that, contrary to expectations, several actors of the cell cycle considered as essential for cell proliferation do not prevent mitotic divisions in development. In this regard, the situation found in the mouse contrasts with the one observed in *Drosophila* (20) and *Caenorhabditis elegans* (9), where cyclin E is absolutely required for normal development. Interestingly, in the mouse, the disruption of some cell cycle regulators appeared to have different phenotypic consequences depending on the tissue or the developmental stage considered. Thus, disruption of Cdk2 does not preclude embryonic and postnatal normal development except for the formation of male and female germ cells, which cannot develop beyond the first meiotic division (2, 37). Therefore, *Cdk2* appears to have a different function in mitotic and meiotic divisions. The E-type cyclin also appears to be dispensable for the development of the embryo proper; however, placental development is severely impaired due specifically to a failure of endoreplicative cycles, characteristic of the trophoblast giant cells (14, 40). Finally, several studies demonstrate that the functions of some cell cycle actors are tissue or cell type specific (reviewed in reference 38). Altogether, these unexpected observations indicate that many aspects of cell cycle regulation during early mammalian embryo development remain to be elucidated.

In the present study, we have characterized a novel mouse gene, *Ovum mutant candidate gene 1* (*Omcg1*), which encodes a nuclear zinc finger protein. We describe its isolation and molecular properties. To investigate its function we have targeted the *Omcg1* locus by homologous recombination in embryonic stem (ES) cells. Disruption of *Omcg1* results in early embryonic lethality at the end of the preimplantation development. Interestingly, *Omcg1*-deficient embryos exhibit alterations of the cell cycle including lengthening of the M phase, abnormal mitotic spindle, and chromosome misalignment. When challenged by nocodazole treatment, the spindle checkpoint was normally activated in mutant embryos. Altogether, these results show that *Omcg1* plays a crucial role in the control of mouse early embryonic cell cycle, which, when perturbed by gene disruption, results in lethality.

MATERIALS AND METHODS

Proteic domain prediction and sequence comparison. Domain predictions of murine OMCG1 protein were done using Smart (http://smart.embl-heidelberg.de/) and PsortII (http://psort.ims.u-tokyo.ac.jp/). The cDNA and the mOMCG1 protein sequences were compared to entries in the EMBL, SwissProt, and GenBank databases using BLAST analysis (http://www.ncbi.nlm.nih.gov/BLAST/). Comparison between protein sequences was performed using ClustalW (47) and depicted using MacBoxshade (http://www.ch.embnet.org/software/BOX_form.html).

Northern blot analysis. Embryo and adult mouse multiple tissue Northern blots from Clontech were hybridized in Hybridexpress buffer (Clontech) with a ^{32}P-labeled probe corresponding to the first 477 bp of *Omcg1* cDNA. Hybridization and washes were performed at 68°C and 50°C, respectively. Autoradiography was performed using X-Omat film (Kodak).

Targeted disruption of the mouse *Omcg1* gene. A 18.3-kb Asp718 129/Sv genomic DNA fragment, containing the single exon *Omcg1* gene, was subcloned from bacterial artificial chromosome CITB-247A17 (accession no. AL713886) (5) and used to generate the targeting vector. It contains 1,555 bp (nucleotides [nt] 12715 to 14270) of the 5′ homology region and 7,434 bp (nt 14536 to 22973) of the 3′ homology region. A fragment encompassing the first 270 bp of the *Omcg1* open reading frame (ORF) was deleted and replaced by a βgeo cassette (12), resulting in the in frame fusion of the βgeo protein with the first three amino acids of OMCG1. A Pgk-DTA cassette encoding the A subunit of the diphtheria toxin gene (provided by P. Soriano) was inserted 5′ to the construct to allow for negative selection in ES cells (51). CK35 ES cells (22) were maintained as previously described (44) in high glucose Dulbecco's modified Eagle's medium supplemented with 15% fetal calf serum, 0.1 mM β-mercaptoethanol, 1 mM sodium pyruvate in the presence of 10^3 U/ml murine leukemia inhibitory factor (LIF). The cells were cultured on mitomicyn C-treated Neo^r primary fibroblasts. A total of 1.6×10^7 CK35 ES cells were electroporated (1 pulse of 0.23 kV and 950 μF) (Gene PulserII; Bio-Rad) with 20 μg of BstBI-linearized targeting vector. After 24 h, G418 (0.3 mg/ml; Invitrogen) was added to culture medium, and resistant ES clones were recovered 10 to 12 days later. Homologous recombination events were identified by Southern blot analysis of genomic DNA (see Fig. 4 for digests and probes). The external probe consisted of a 900-bp fragment mapping 4.3 kb 5′ to the *Omcg1* transcriptional start, while the internal probe corresponded to the 3′ half of the ORF. Two correctly targeted ES clones that were shown to carry single copy integration at the *Omcg1* locus were injected into C57BL/6N blastocysts. The resulting chimera males were then mated with C57BL/6N and 129/Sv females, and germ line transmission of the targeted *Omcg1* locus was confirmed by PCR using primers 1 (5′-ACTCGCCTGAGTC CTGGGCGC), 4 (3′-ATGGGCGCATCGTAACCGTGC), and 5 (3′-GGCAG TAAACCGAGTCCAGGT).

Early embryo isolation and in vitro culture. Heterozygous *Omcg1*$^{+/-}$ females were superovulated by injection of 5 units of pregnant mare serum gonadotrophin (Calbiochem), followed by injection of 5 units of human chorionic gonadotrophin (Intervet) 48 h later, and then crossed with heterozygous *Omcg1*$^{+/-}$ males. The next day, successful matings were detected by the presence of a vaginal plug. Embryos at different stages of development (embryonic day 0.5 [E0.5] through E2.5) were collected by either dissecting ampullae or flushing oviducts with PB1 medium (50). E3.5 blastocysts were collected by flushing uteri with ES cell medium without LIF and supplemented with 20 mM HEPES. For in vitro culturing, blastocysts were placed (possibly after zona pellucida removal by acidic Tyrod's solution treatment) individually for 24 h (E4.5) to 3 days in ES cell medium without LIF onto 0.1% gelatin-coated chambered coverglass (Lab-Tek) and photographed every 24 h (Leica DMIL and Nikon Coolpix990). For drug treatment, culture of pooled E4.5 embryos was followed by 7 h of incubation in medium containing 5 μg/ml mitomycin C (Fluka) or 3 h of incubation in medium containing 2.5 μM nocodazole (Sigma).

Immunofluorescence. Embryos were fixed for 10 min at room temperature with 4% paraformaldehyde and then permeabilized for 10 min at room temperature with 0.25% Triton X-100. Incubations with primary and secondary antibodies were performed in phosphate-buffered saline (PBS), 0.1% Tween-20, and 10% fetal calf serum. The following antibodies were used: anti-bromodeoxyuridine ([BrdU] 1:100; Roche), anti-cytokeratin-endoA antibody (TROMA-1 at 1:100; DSHB clone SP2/0), anti-hemagglutinin antibody (1:1,000) (clone 16B12; Covance), anti-Oct-3/4 antibody (OCT-3/4 at 1:300; BD Biosciences), anti-OMCG1 (1:300), anti-phospho-histone H3 antibody (HH3ser10P at 1:100; Upstate), anti-α-tubulin antibody (1:2,000; clone B-5-1-2; Sigma), anti-γ-tubulin antibody (1:200; Sigma), Alexa 488-nm anti-rabbit (1:100; Molecular Probes) and Alexa 594-nm anti-mouse antibody (1:200; Molecular Probes). Embryos were incubated at room temperature for 90 min with primary antibodies and for 1 h with secondary antibodies. Nuclei were counterstained with DAPI (4′,6′-diamidino-2-phenylindole) or Hoechst 33342 (Sigma) stain, and embryos were mounted individually in Immuno-Fluore mounting medium (MP Biomedicals). Fluorescent images were obtained using a confocal laser scanning microscope (LSM510 and FCS; Zeiss) or fluorescence microscope (Axioplan 2 imaging; Zeiss) equipped with a digital camera (Axiocam Mrm; Zeiss). To determine the number of mitotic cells, we counted cells positive for HH3ser10P immunostaining. As it is difficult to distinguish cells in late G_2 phase from cells in early prophase, only cells in prometaphase to telophase stages were counted. Immunofluorescence with anti-MAD2 antibody (a generous gift from Katja Wassmann) was performed according to Wassmann et al. (49).

Generation of rabbit anti-OMCG1 antisera. A recombinant fusion protein of the OMCG1 protein was produced in *Escherichia coli* as a glutathione transferase fusion protein from a pGEX-4T1 expression vector (Pharmacia Biotech) and purified using a glutathione-conjugated affinity column (Pharmacia Biotech). Purified protein was then used as an immunogen for the production of rabbit antiserum (Agro-Bio, France).

TUNEL assay. DNA fragmentation-associated cell death was detected by a terminal deoxynucleotidyltransferase (TdT)-mediated dUTP-fluorescein nick end labeling (TUNEL) assay using an In Situ Cell Death Detection kit Pod (Roche). In brief, E4.5 blastocysts were fixed in 4% paraformaldehyde and permeabilized for 10 min at room temperature in PBS, 0.1% Triton X-100, 0.1% sodium citrate. Embryos were washed several times in PBS-bovine serum albumin (6 mg/ml) and then incubated with digoxigenin-dUTP and terminal deoxynucleotidyltransferase enzyme for 1 h at 37°C. After several washes in PBS-bovine serum albumin, embryos were observed under a fluorescence microscope and genotyped by PCR.

BrdU labeling of cultured blastocysts. E4.5 blastocysts were cultured in ES cell medium without LIF containing 10 mM BrdU (Roche) for 2 h. Embryos were then fixed in 4% paraformaldehyde for 10 min, permeabilized for 10 min in 0.25% Triton X-100, and treated with 2N HCl for 10 min at room temperature, after which immunofluorescence was performed as described below.

Genotyping embryos by nested PCR. After analysis, embryos were lysed into 10 μl of lysis buffer (10 mM Tris, pH 8.5, 50 mM KCl, 0.01% gelatin, 300 μg/ml proteinase K) in a Hybaid express PCR machine (50°C for 50 min; 90°C for 10 min). Five microliters of lysate was used for the first round of PCR in a total volume of 50 μl using a mixture of three primers: 1, 2 (3′-ACAACCCGTCGG ATTCTCCGT), and 3 (3′-AATGAGGAACTAAGGGGGCCT). The PCR amplification protocol consisted of an initial incubation at 94°C for 5 min, followed by 25 cycles at 94°C for 30 s, 58°C for 60 s, and 72°C for 60 s, with a final incubation at 72°C for 5 min. A total of 5 μl of the first PCR was used for the second round of PCR amplification for 20 cycles with a mixture of the three primers 1, 4, and 5.

Nucleotide sequence accession number. The sequence corresponding to the 3′ end of the *Omcg1* transcript was derived from a DDK oocyte cDNA and has been submitted to the GenBank/EBI Data Bank under accession number AY786540.

RESULTS

Identification of *Omcg1* gene coding for a conserved zinc finger protein. During the positional cloning of the *Ovum mutant* locus involved in a conditional preimplantation lethality phenotype (1, 5, 24), we isolated a novel murine gene which we called *Ovum mutant candidate gene 1*. *Omcg1* partial cDNAs were obtained by cDNA hybridization/selection of DDK oocyte cDNA onto bacterial artificial chromosome CITB-49L3 from the ovum mutant region (5). Database searches revealed that *Omcg1* corresponds to the previously uncharacterized RIKEN cDNA 2410003C20 gene (GeneID 66983). Figure 1A shows the structure of a 2,441-nt mRNA corresponding to the NM_025884 RefSeq mRNA extended by 98 nt in its 3′ end (Fig. 1A, dashed underlining). It is likely that this added region represents the true 3′ end of *Omcg1* transcripts because of the following: (i) it was found in our *Omcg1* partial cDNAs as well as in several expressed sequence tags, (ii) two consensus AA UAAA polyadenylation signals are present in the added region, and (iii) the NM_025884 RefSeq mRNA 3′ end is flanked by an A-rich region that might have been used as an internal priming site during an oligo(dT)$_n$ reverse transcription step. In silico analysis revealed the existence of two shorter *Omcg1* transcripts, spanning 1,287 and 1,578 nt, respectively, and differing by the length of their 3′ untranslated region (UTR) (Fig. 1A, arrowheads). We noticed in the 3′ UTR the presence of several posttranscriptional elements such as deadenylation signals and oocyte-specific cytoplasmic polyadenylation elements (Fig. 1A, underlined). Differential distribution of these elements in the three *Omcg1* transcripts (Fig. 1B) suggests that they may have different stability and/or translation properties, in particular in oocytes and during preimplantation development. The 5′ UTR of *Omcg1* transcripts is 22 bases long and is followed by an ORF of 1,092 bases. This ORF codes for a 40.3-kDa protein composed of 363 amino acids. Computer-based structural analysis of the ORF predicted that the protein contains a single C_2H_2 zinc finger motif (amino acids [aa] 53 to 75), two bipartite nuclear localization signals (aa 22 to 38 and 102 to 118), a short stretch of negatively charged glutamic acid (E) and aspartic acid (D) residues (aa 154 to 162), and two coiled-coil domains (aa 13 to 40 and 269 to 340) in the amino- and carboxy-terminal regions, respectively (Fig. 1B).

Searches through protein sequence databases yielded uncharacterized or hypothetical OMCG1-related proteins from several species including human, rat, zebrafish, fruit fly, and nematode but not yeast. Alignments of orthologous OMCG1 proteins showed a high degree of conservation (Fig. 2). Rat and human OMCG1 have 92% and 84% overall identity with mouse OMCG1, respectively. Most differences between the three mammalian orthologous proteins are clustered in the central region of the protein (Fig. 2A, underlined). This central region is missing in *C. elegans* and fruit fly proteins. It should be noted that in these two species, the zinc finger domain is not predicted because of a missing residue between the cysteine and histidine residues.

***Omcg1* codes for a widely expressed nuclear protein.** Analysis of tissue expression of *Omcg1* showed that it was expressed in many tissues but at low levels. Northern blot analysis revealed three RNA species of about 1.3, 1.5, and 2.5 kb (Fig. 3A). The smaller transcript was detected only in the testis and at a higher level than the other RNA species. Sequence alignments between *Omcg1* transcripts and expressed sequence tags from the Mm.29622 cluster indicated that the short transcript was also expressed in sympathetic ganglia and the preimplantation embryo. The two other transcripts were expressed at low levels in all adult tissues and in embryos at various stages.

To investigate the subcellular distribution of OMCG1 protein, we constructed vectors expressing the full-length protein fused at its C terminus either to green fluorescent protein or hemagglutinin tag and then electroporated them into HeLa cells. We observed that the fusion proteins were uniformly distributed within the nucleus but were excluded from the nucleoli (see Fig. S1 in the supplemental material). Using an anti-OMCG1 antibody, we observed a nuclear distribution of the endogenous protein in ES cells and preimplantation mouse embryos (Fig. 3B) (see Fig. 6A; and see also Fig. S1 in the supplemental material). Interestingly, in metaphase II oocytes and in mitotic blastomeres, OMCG1 was detected in the cytoplasm, indicating that the protein was not associated with chromosomes during mitosis or, if associated, was not accessible to antibodies.

Targeting *Omcg1* in ES cells and its requirement for their survival. To determine the function of *Omcg1*, we disrupted the gene by homologous recombination in ES cells. *Omcg1* contains only one exon (Fig. 4A). We generated a targeting vector in which the coding sequence of a LacZ reporter/neomycin phosphotransferase selector gene (βgeo) was inserted in frame with the three first amino acids of OMCG1 (Fig. 4A). CK35 ES cells were electroporated with the targeting vector with or without a negative selection cassette. Correctly targeted

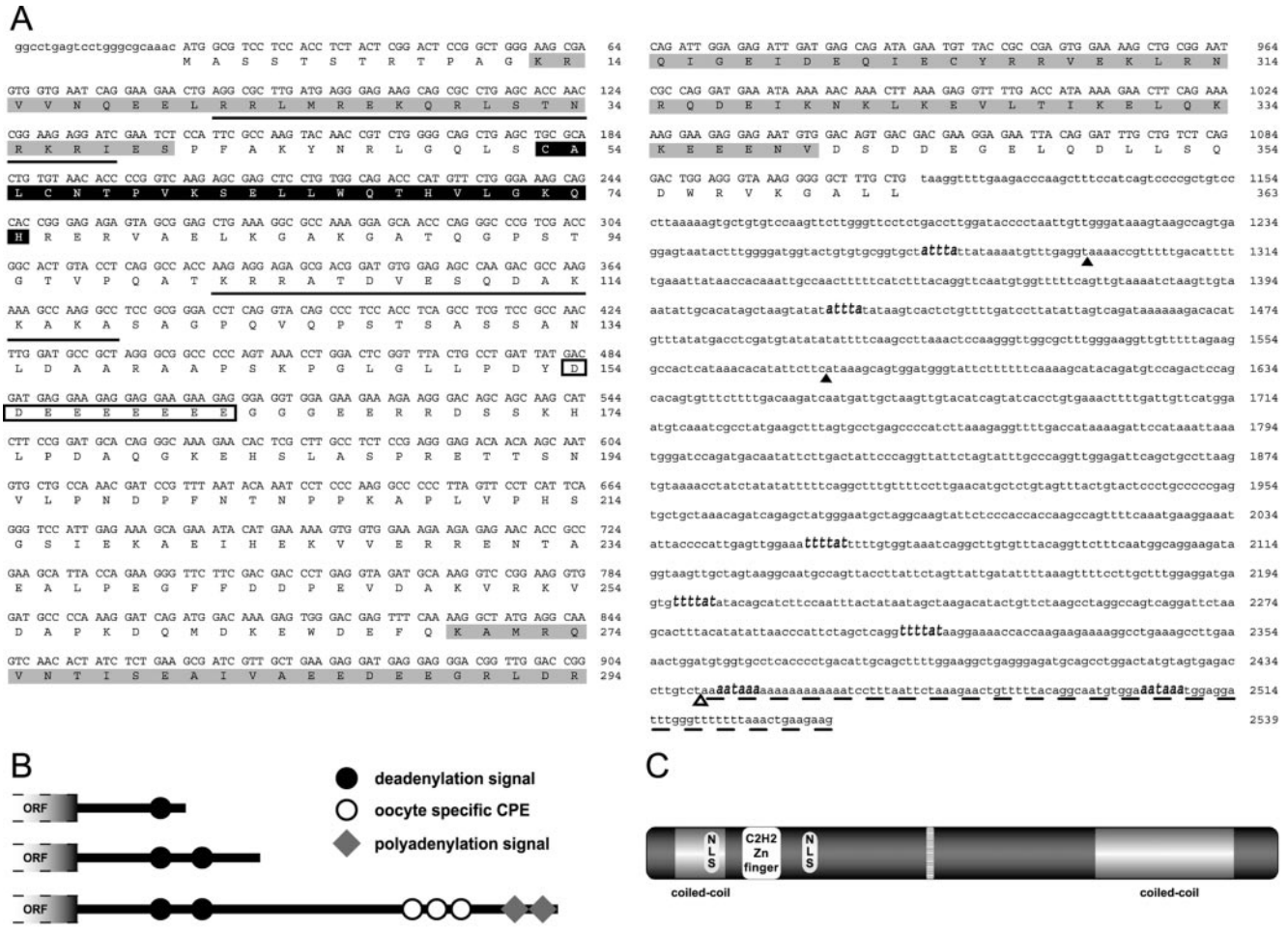

FIG. 1. *Omcg1* transcripts and protein structure. (A) Nucleotide and predicted amino acid sequence of mouse *Omcg1* cDNA. Nucleotide sequence corresponds to *Omcg1* mRNA RefSeq NM_025884; sequences 3′ of nt 2441 (empty arrowhead) have been derived from a DDK oocyte cDNA (dashed underlining). Sequence data for this additional sequence are available from GenBank/EMBL/DDBJ under accession no. AY786540. The black arrowheads point to the 3′ end of *Omcg1* shorter transcripts: AK017640 (1,287 nt) and AK008475 (1,578 nt). The deadenylation signal (attta), oocyte-specific cytoplasmic polyadenylation element (ttttat), and polyadenylation signal (aataaa) are indicated in bold italic. The coiled-coil and zinc finger domains are shadowed in gray and black, respectively. Putative bipartite nuclear localization signals (NLS) are indicated by solid underlining. The short stretch of negatively charged residues is boxed. (B) Schematic representation of the 3′ UTR of the three *Omcg1* transcripts. (C) Schematic representation of OMCG1 protein.

clones were identified by Southern blot analysis (Fig. 4B and D). We also attempted to inactivate both *Omcg1* alleles in ES cells. We first used the approach of Mortensen et al. which relies on the higher resistance to selection of the homozygous targeted clones (34); however, no *Omcg1*$^{-/-}$ clones could be recovered when singly targeted clones were cultured in high concentration of G418 (unpublished data). We thus tried to target the wild-type allele of the *Omcg1*$^{+/-}$ ES cells, with a vector in which the βgeo selector gene was replaced by a puromycin resistance cassette. Although puromycin-resistant homologous recombinants were identified, the recombination took place systematically with the previously targeted allele. When selection was applied for both markers, only random integrants were isolated (Fig. 4D). We concluded from these experiments that *Omcg1* is essential for maintenance and/or survival of ES cells.

***Omcg1* is essential for preimplantation development.** We injected modified ES cells into C57BL/6 blastocysts and obtained germ line transmission of the *Omcg1*-targeted allele for two independent ES clones. The phenotype described below was observed in animals derived from both clones and was fully penetrant on mixed (129/Sv × C57BL/6) and pure 129/Sv genetic backgrounds. Both *Omcg1*$^{+/-}$ males and females were normal and fertile and transmitted the targeted allele to about 50% of their progeny. However, no homozygous *Omcg1*-deficient offspring were born from heterozygous intercross matings (Table 1), indicating that *Omcg1* homozygous deficiency causes embryonic lethality. An analysis of E6.5 and E10.5 embryos revealed that none of the 89 embryos genotyped were *Omcg1* null. However, the expected Mendelian frequency of heterozygote, homozygote null, and wild-type blastocysts was observed in E3.5 embryos. It is noteworthy that we did not observe a higher rate of E6.5 empty or resorbed deciduas in heterozygous intercrosses compared to control crosses (unpublished data). We concluded from these observations that *Omcg1*-deficient embryos died at the peri-implantation period and failed to implant into the uterine wall.

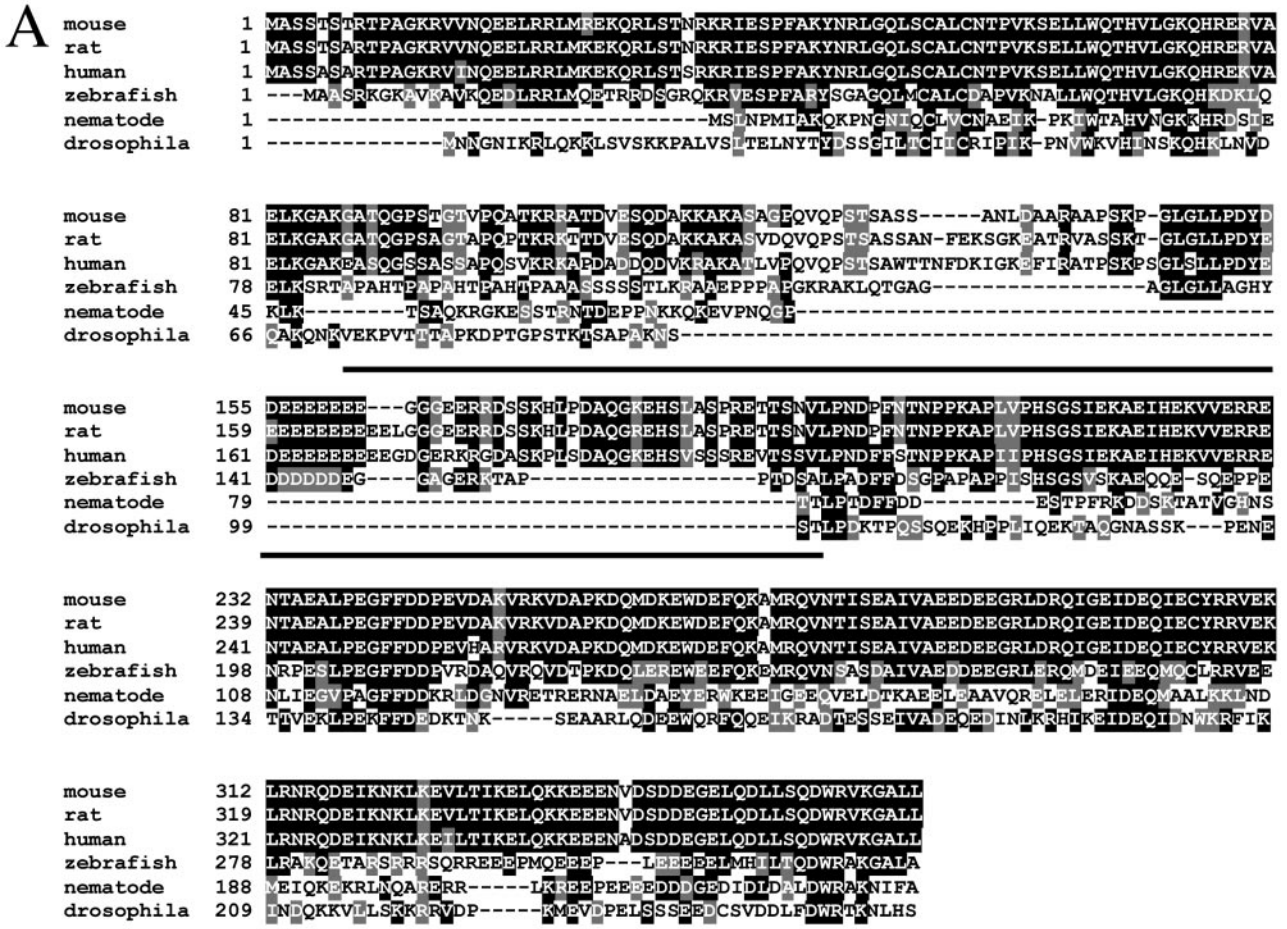

FIG. 2. Comparison between OMCG1 and its orthologous proteins. (A) Sequence comparison of OMCG1 and related proteins. *Homo sapiens* (human), accession no. BAB70992; *Rattus norvegicus* (rat; protein sequence was determined from conceptual translation of the rat genomic locus, identified by sequence alignment of the mouse cDNA with rat genomic sequence, clone CH230-105H4), accession no. AC128344; *Danio rerio* (zebra fish), accession no. AAH65604; *C. elegans* (nematode), SwissProt accession no. Q22139; and *D. melanogaster* (drosophila), accession no. AAF56392. Identical amino acid residues are shaded black, similar residues are shaded gray, and different residues are not shaded. Intermediate part of OMCG1 (underlined) is poorly conserved. (B) Percentage of sequence identity between related proteins.

To analyze in more detail the phenotype of *Omcg1*$^{-/-}$ embryos, E3.5 blastocysts from intercrosses were cultured individually for 3 days and then genotyped. Under these conditions, wild-type and heterozygous embryos hatched from their zona pellucida and attached onto the culture dish; the ICM expanded and outgrew, while the trophectoderm layer became adherent and differentiated into giant cells (Fig. 5A). In contrast, most *Omcg1*-null embryos (16/23) were unable to hatch (Fig. 5B). Among the seven mutant embryos that hatched, only two attached to the dish (Fig. 5C). In all cases, *Omcg1*-deficient blastocysts failed to expand or proliferate and degenerated rapidly. Removal of the zona pellucida prior to the culture gave similar results except that, for the embryos that attached to the substrate (5/9), a few trophectodermal cells were able to spread before degenerating. Interestingly, these cells were plurinucleated (Fig. 5E, arrows). These data demonstrate that blastocyst outgrowth in vitro is severely impaired in the absence of *Omcg1* due to failure of the growth of both ICM and trophectoderm.

Cell cycle defects in *Omcg1*-deficient embryos. The lethality of *Omcg1*$^{-/-}$ embryos at the peri-implantation period could reflect a critical role for *Omcg1* at that time. Alternatively, maternally supplied *Omcg1* mRNA and protein stores could conceal in the knockout embryos an earlier function of this gene. To distinguish between these two possibilities, we performed OMCG1 immunostaining on E3.5 intercross blasto-

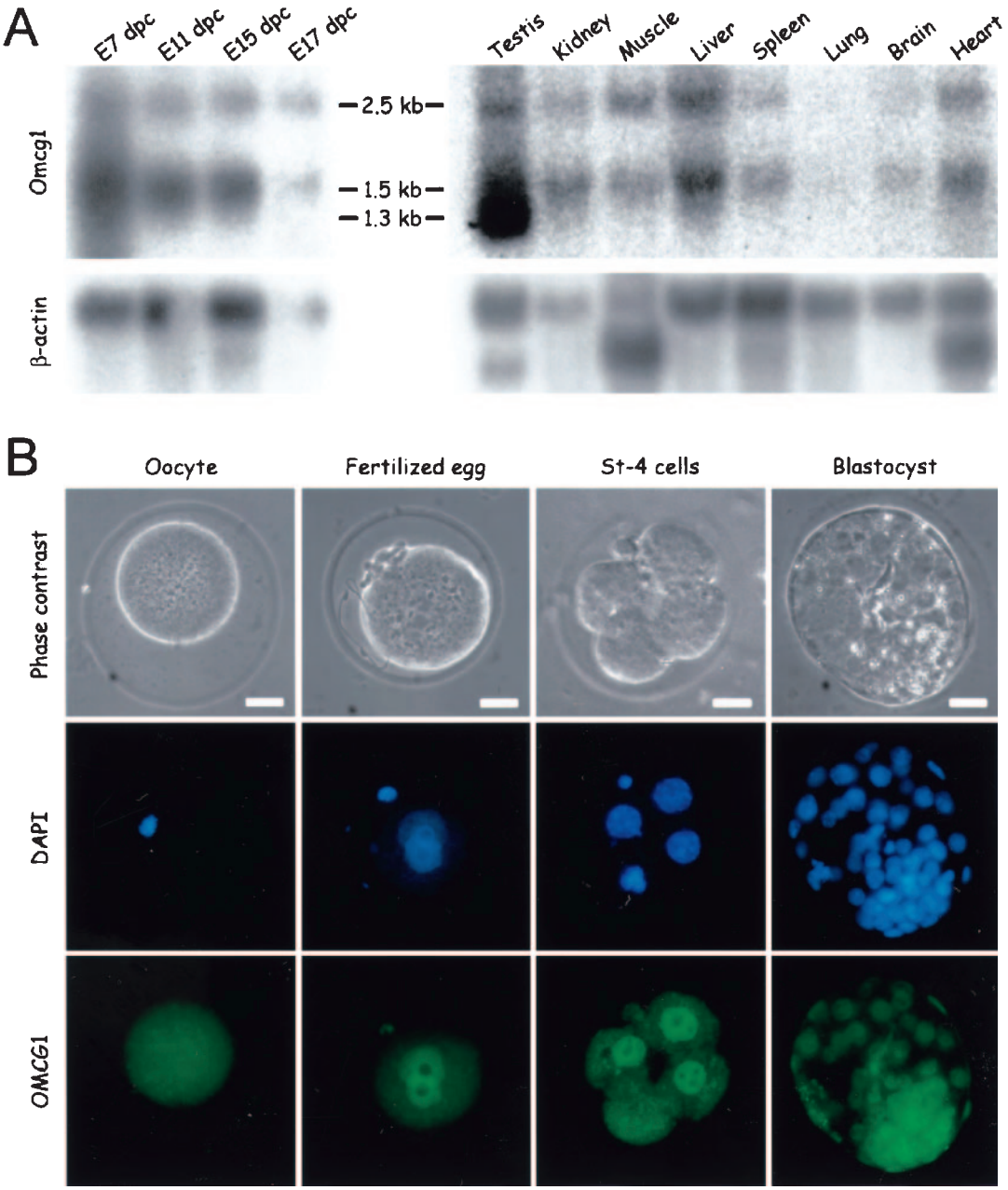

FIG. 3. Expression of *Omcg1* in adult and preimplantation embryo. (A) Northern blot analysis of poly(A)$^+$ mRNA of E7.5 to E17.5 embryos and of various adult tissues probed with an *Omcg1*-specific probe (upper panels) or a β-actin probe (lower panels). (B) OMCG1 immunodetection in metaphase II oocytes and early embryos. Bar, 30 μm.

cysts and E3.5 intercross blastocysts cultured for 24 h in vitro (called hereafter E4.5). As shown in Fig. 6A, by E3.5 nuclear OMCG1 immunostainning was present in *Omcg1*$^{-/-}$ cells, while it was no longer discernible 24 h later (see also Fig. S2 in the supplemental material). Therefore, the developmental arrest of *Omcg1*$^{-/-}$ embryos appeared to be correlated with the loss of OMCG1 protein.

To analyze the phenotype of *Omcg1*-null blastocysts before they die, we decided to look at E4.5 late blastocysts, i.e., by the time the maternal protein is no longer present. First, we performed immunofluorescence analysis of *Omcg1* heterozygous intercross embryos using ICM-specific (OCT-3/4) and trophectoderm-specific (TROMA-1) markers. As expected, wild-type and heterozygous embryos gave strong nuclear OCT-3/4-positive and cytoplasmic TROMA-1-positive signals in the ICM and the trophectoderm, respectively (Fig. 6B). Similar immunostaining was observed in *Omcg1*$^{-/-}$ embryos, suggesting that the developmental arrest of these embryos was not due to a lack of differentiation of early embryonic lineages.

While E3.5 *Omcg1*$^{-/-}$ blastocysts were indistinguishable from their littermates (wild type or *Omcg1*$^{+/-}$), about 30% of E4.5 *Omcg1*$^{-/-}$ embryos could be recognized by phase-con-

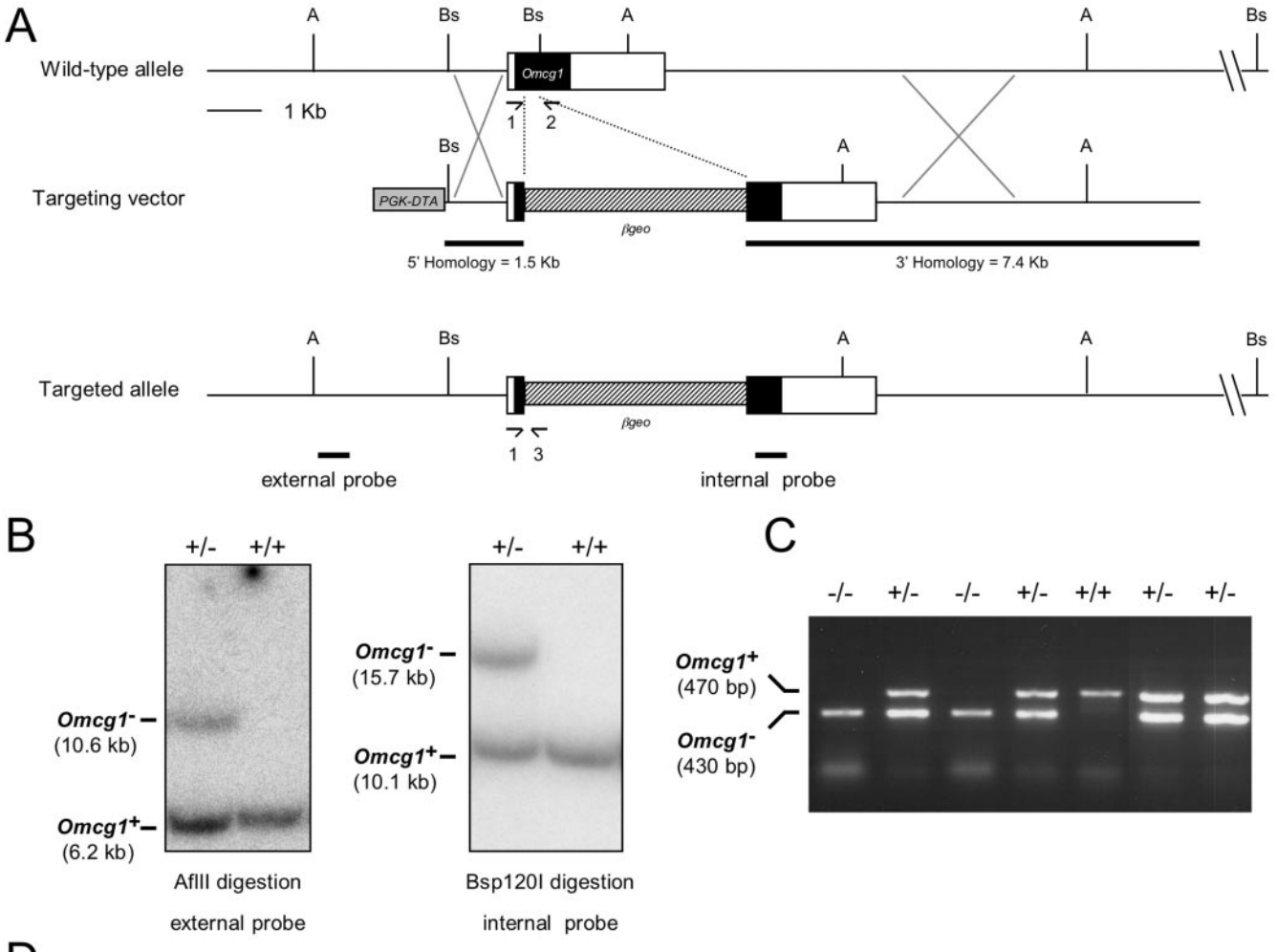

D

(1) Introduction of *Omcg1* - βgeo targeting vector into CK35 ES cells

Targeting vector	Selection	Analysed colonies	Integration event: Random	Integration event: Targeted
Omcg1 - βgeo without DT-A	G418	100	83	17
Omcg1 - βgeo with DT-A	G418	52	6	46

(2) Introduction of *Omcg1* - PGKpuro targeting vector into ES cells heterozygous for *Omcg1* - βgeo allele

Targeting vector	Selection	Analysed colonies	Integration event: Random	Integration event: Retargeted	Integration event: 2nd allele
Omcg1 - PGKpuro	Puro	48	44	4	0
Omcg1 - PGKpuro	Puro + G418	108	108	0	0

FIG. 4. Targeted disruption of *Omcg1* gene. (A) Schematic diagram showing the *Omcg1* wild-type locus, the targeting vector, and the targeted allele. Black boxes represent *Omcg1* ORF, while white boxes represent the 5′ and 3′ UTRs. The hatched boxes represent the βgeo cassette, and the gray box represents the Pgk-DTA cassette used for negative selection. Arrows 1 to 3 indicate the positions and the orientations of PCR primers used for genotype analysis in panel C. External and internal probes used in panel B are shown as solid bars beneath the targeted allele. Restriction enzymes: A, AflII; Bs, Bsp120I. (B) Southern blot analysis of genomic DNA obtained from wild-type and heterozygous ES cells. (C) Genotyping analysis of E4.5 embryos recovered from $Omcg1^{+/-}$ heterozygous intercrosses. A 470-bp band is amplified from wild-type allele by primers 1 and 2, whereas a 430-bp is amplified from targeted allele by primers 1 to 3. (D) *Omcg1*-targeting constructs were electroporated into CK35 $Omcg1^{+/+}$ cells or $Omcg1^{+/-}$ ES cells. After selection, resistant clones were analyzed by Southern blotting and/or by PCR to determine their genotypes.

trast microscopy since they generally had a small and globular ICM that was not closely apposed to the trophectoderm (Fig. 5B, star). In addition, trophectodermal cells appeared larger than in control embryos, suggesting that *Omcg1*-null embryos are composed of fewer cells (Fig. 5B, white arrow). To confirm this point, we counted the number of nuclei by DAPI staining of E4.5 intercross embryos (Fig. 7A). Whereas $Omcg1^{+/+}$ and $Omcg1^{+/-}$ blastocysts contained a

TABLE 1. Genotype analysis of *Omcg1*$^{+/-}$ intercross progeny

Stage	No. of embryos by genotype[a]			Total no. of embryos
	+/+	+/−	−/−	
Postnatal	41	72	0	113
E10.5	11	22	0	33
E6.5	13	43	0	56
E3.5	31	55	23	109

[a] Genotype analysis of *Omcg1* heterozygous intercross progeny. Embryos were genotyped by nested PCR for E3.5 and by PCR for the other stages.

similar number of cells (respectively, 85.4 ± 17.9 nuclei [n = 23] and 83.4 ± 16.9 nuclei [n = 46]), the number of DAPI-stained nuclei was reduced in *Omcg1*$^{-/-}$ blastocysts (57.6 ± 17.5 nuclei; n = 26). This reduction of about 30% is statistically significant (n = 95; $P < 0.0001$ by analysis of variance [ANOVA]).

We then investigated whether the reduction of cell number was a result of increased cell death, decreased cell proliferation, or both. A TUNEL assay was performed on E4.5 intercross blastocysts (Fig. 7B). A slight increase in the number of TUNEL-positive cells was observed in *Omcg1*$^{-/-}$ compared to *Omcg1*$^{+/+}$ and *Omcg1*$^{+/-}$ embryos. However, this difference was not significant (n = 40; $P = 0.0851$ by ANOVA), indicating that apoptosis was not the main cause for the reduction in cell number in *Omcg1*$^{-/-}$ embryos. We then used histone H3 phosphorylation on the serine 10 residue to determine the number of cells in M phase. Phosphorylation of histone H3 has been shown to correlate with chromosome condensation during mitosis (17) and to constitute a specific marker of mitotic cell from prophase to early telophase. Strikingly, whereas the number of mitotic cells was similar in *Omcg1*$^{+/+}$ and *Omcg1*$^{+/-}$ embryos (respectively, 2.8 ± 1.9 cells [n = 31] and 2.5 ± 2.2 cells [n = 80]), it increased by approximately threefold in *Omcg1*-deficient embryos (7.7 ± 5.2 cells; n = 38) (Fig. 7C). This increase was statistically significant (n = 159; $P < 0.0001$ by ANOVA). Altogether, these observations suggest that *Omcg1*-null embryos are severely affected in their ability to progress appropriately through the cell cycle.

Abnormal mitosis in *Omcg1* mutant embryos. The observation that *Omcg1*$^{-/-}$ embryos have an increased mitotic index together with a reduced total number of cells led us to analyze in more detail the cell cycle in these embryos. E4.5 blastocysts were treated with BrdU for 2 h, and incorporation of BrdU into DNA during S phase was monitored by indirect immunofluorescence using an anti-BrdU antibody. After fixation, embryos were placed into an acidic solution in order to improve the accessibility of anti-BrdU antibody to DNA. However, we found that such treatment was not compatible with embryo genotyping. Embryos were therefore classified based on their number of mitotic cells. Indeed, we previously noticed that more than 80% of E4.5 embryos with seven or more mitotic cells were *Omcg1*$^{-/-}$, whereas only 11% of *Omcg1*$^{-/-}$ embryos had three or fewer mitotic cells. With wild-type and heterozygous embryos, the inverse was observed (unpublished data). Thus, we compared the number of BrdU-positive cells between these two categories of embryos (Fig. 8A) (respectively, 47.8 ± 4.8 cells [n = 6] and 53.7 ± 10.8 cells [n = 32]). A similar number of BrdU-positive cells was observed in both categories (n = 38; $P = 0.1962$ by ANOVA), indicating that at this stage *Omcg1*$^{-/-}$ cells are actively cycling.

The increased mitotic index of *Omcg1*$^{-/-}$ embryos could result from a block in mitosis or a lengthening of the duration of the M phase. To discriminate between these two possibilities, E4.5 blastocysts were treated for 7 h with mitomycin C, an agent which cross-links adjacent guanines and so blocks cells in S or G_2 phases in response to the activation of the DNA damage checkpoint (19). As shown in Fig. 8B and C, mitomycin C treatment induced a statistically significant diminution of the number of mitotic cells in wild-type (n = 82; $P < 0.0007$ by ANOVA) and heterozygous embryos (n = 141; $P < 0.005$ by ANOVA). A similar effect of mitomycin C treatment on the number of mitotic cells was observed in *Omcg1*$^{-/-}$ embryos (n = 62; $P < 0.005$ by ANOVA), suggesting that mitomycin C treatment effectively induced cell cycle arrest before mitosis and that *Omcg1*-deficient cells were not blocked in M phase. The latter conclusion is strengthened by the observation that the number of mitotic cells in *Omcg1*$^{-/-}$ embryos did not increase when E4.5 blastocysts were cultured for 7 h in the absence of mitomycin C (Fig. 8B and C, None).

By microscopic examination of HH3ser10P-stained *Omcg1*$^{-/-}$ embryos, we noticed the presence of abnormal mitotic figures such as scattered metaphase plates or isolated chromosomes. Therefore, we looked at the distribution of chromosomes in relation to the mitotic spindle and centrosomes by immunofluorescence using anti-α-tubulin, anti-γ-tubulin, and anti-HH3ser10P antibodies. Normal mitoses were observed in *Omcg1*-null embryos (Fig. 9A and D). However, in most deficient embryos, we observed one or several anomalies in the organization of the mitotic spindle and the position of chromosomes, such as tripolar mitotic spindles (Fig. 9B), misalignment between metaphasic plate and spindle (Fig. 9C), or isolated chromosomes generally connected to a single pole of the spindle (Fig. 9C, asterisk). An abnormal number of centrosomes was often observed in multipolar spindle figures (Fig. 9E and F). Such abnormal mitotic figures were not observed in wild-type and heterozygous embryos.

Given that abnormal mitotic spindles were observed in mutant embryos, we asked whether the mitotic checkpoint, which normally ensures that chromosomes are properly attached to the spindle before sister chromatid separation occurs in anaphase, is functional in the absence of *Omcg1*. E4.5 blastocysts were incubated with 2.5 μM nocodazole for 3 h. As expected, this treatment induced a mitotic block in wild-type and heterozygous embryos, as evidenced by the great increase in the number of mitotic cells (Fig. 8B and C) (from 2.8 ± 1.9 to 14.1 ± 2.7 cells and from 2.5 ± 2.2 to 14.3 ± 7.4 cells, respectively). In *Omcg1*-deficient embryos, the number of mitotic cells varied from 7.7 ± 5.3 cells (n = 38) without treatment to 14.0 ± 3.0 cells (n = 7) after nocodazole treatment (Fig. 8B and C). This variation is statistically significant (n = 45; $P < 0.0001$ by Fisher's test). Although the increase in the number of mitotic cells in null embryos appears modest when compared to wild-type and heterozygous embryos, it represents about 14% of the cell mean number, as it does in the other categories of embryo. To confirm the spindle checkpoint functionality, we monitored MAD2 localization in mitotic cells. MAD2 protein is involved in the spindle assembly checkpoint (27), which links chromosome-microtubule attachment to the metaphase-anaphase

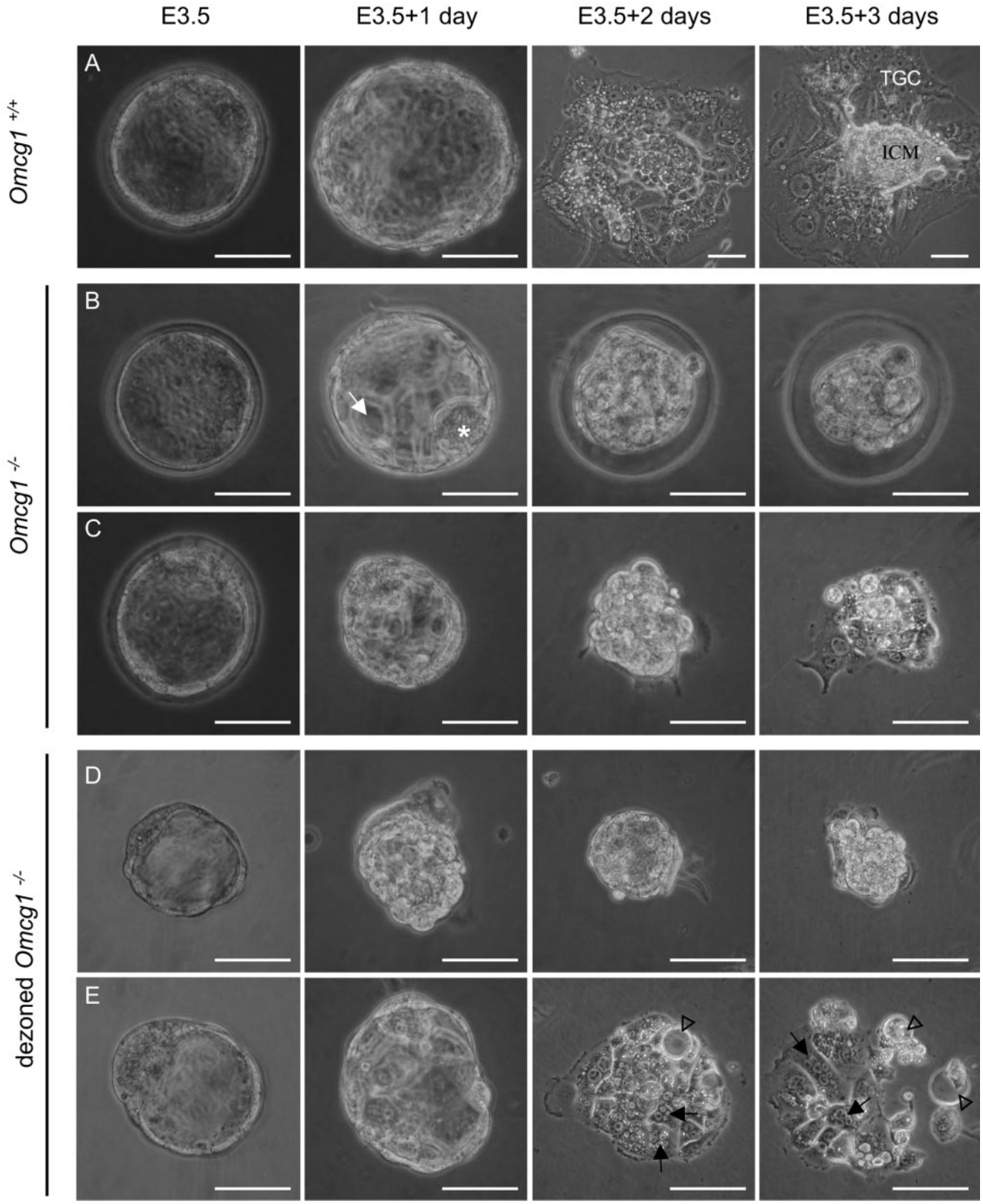

FIG. 5. Aberrant blastocyst outgrowths of *Omcg1*$^{-/-}$ embryos. E3.5 blastocysts from *Omcg1* intercrosses were cultured in vitro and photographed every 24 h using phase-contrast microscopy. At the end of the culture, each embryo was recovered and genotyped by nested PCR. Wild-type (A) and heterozygous blastocysts hatched from their zona pellucida after 1 day and attached to the culture dish. After 3 days in culture, outgrowths were composed of the inner cell mass surrounded by a single layer of trophectoderm giant cells (TGC). *Omcg1*-deficient embryos either failed to hatch (B) or, when they did, failed to proliferate (C). After 1 day in culture, some were composed of larger trophectoderm cells (white arrow) and a small globular ICM (asterisk in panel B). (D and E) Two examples of the culture of chemically dezoned null blastocysts. The first one (D) attached but failed to spread on the dish and to proliferate; the second one (E) also attached to the dish but, after 2 days in culture, most cells were degenerating (empty arrowheads), while a few plurinucleated cells could still be seen (black arrows).

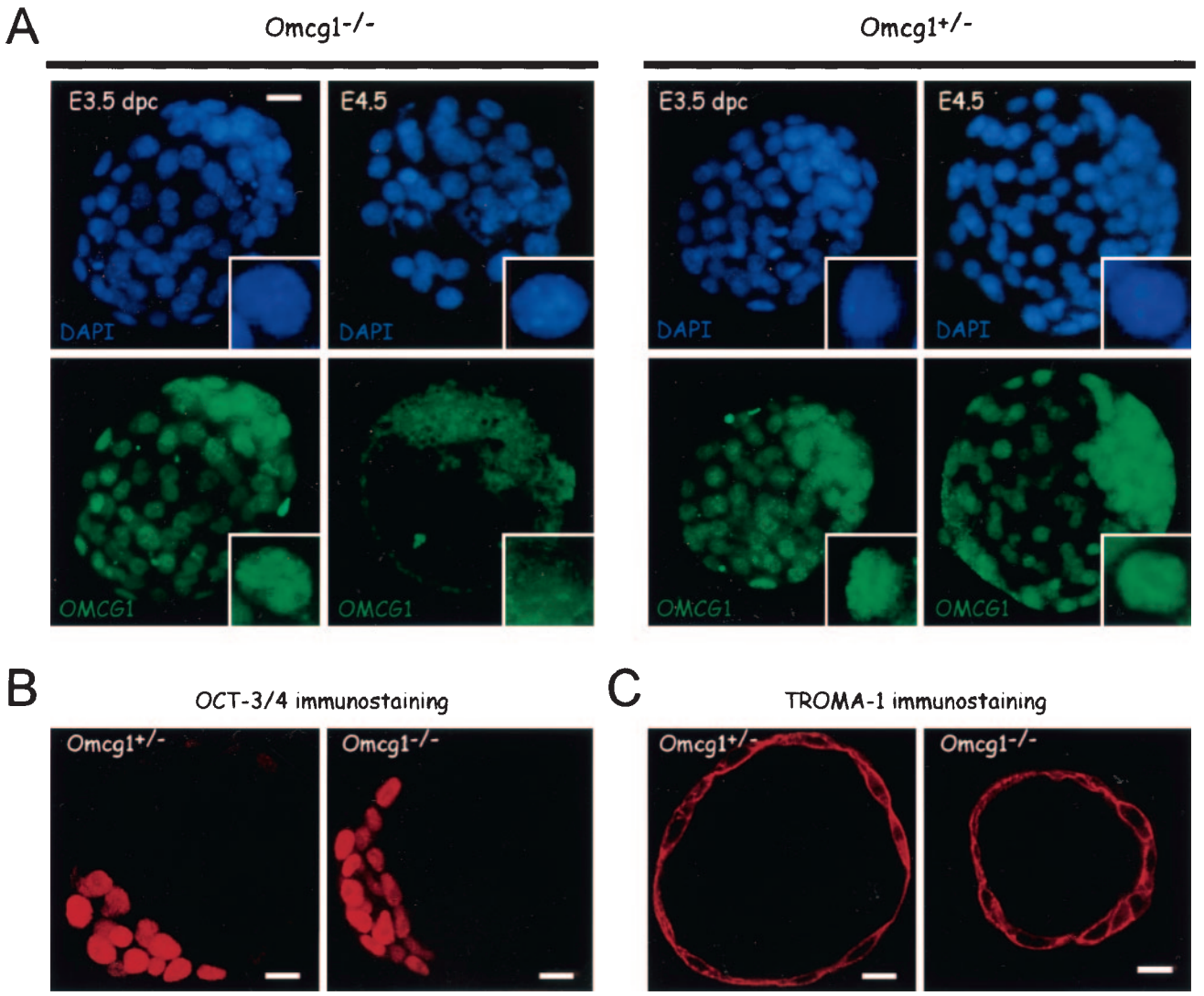

FIG. 6. OMCG1, OCT-3/4, and TROMA-1 distribution in *Omcg1*$^{+/-}$ and *Omcg1*$^{-/-}$ blastocysts. (A) Immunodetection of OMCG1 protein in E3.5 and E4.5 *Omcg1*$^{+/-}$ and *Omcg1*$^{-/-}$ blastocysts. OMCG1 nuclear signal is present in E3.5 embryos but disappears in E4.5 null embryos. Nuclei were counterstained by Hoechst 33342. Embryos were observed under a fluorescence microscope. Insets show higher magnifications of a single cell. (B and C) Immunodetection of two markers of cell lineages in E4.5 embryos from *Omcg1*$^{+/-}$ intercrosses: OCT-3/4 and TROMA-1 are expressed in ICM (B) and TE (C), respectively. Embryos were observed by confocal microscopy. In panel B, images show a medial orientation of a three-dimensional reconstruction. After analysis, embryos were individually recovered and genotyped. Bar, 20 μm.

transition (43). It was shown to localize on the kinetochores unattached to microtubules (29). Immunofluorescence analysis revealed that, upon nocodazole treatment, MAD2 is detected on kinetochores in mitotic cells not only in wild-type and heterozygous embryos but also in null embryos (Fig. 8D). In untreated embryos, MAD2 localization to kinetochores was observed in a few mitotic cells (Fig. 8D). No difference in its distribution was detected in null E4.5 blastocysts compared to wild-type and heterozygous embryos. Altogether, these experiments demonstrate that the mitotic spindle checkpoint is functional in E4.5 *Omcg1*-deficient embryos.

Postranslational modifications of histones are not responsible for mitosis lengthening. Posttranslational modifications of histones contribute to driving changes in chromatin conformation and compaction. Acetylation and methylation of the amino-terminal tails of histones are generally associated to the active or repressed transcriptional states, respectively (for a review, see reference 10). In mitotic cells, an overall reduction in acetylated H3 and H4 histones has been observed compared with interphase nuclei (23). Moreover, the maintenance of a hyperacetylated histone state in mitosis induces improper chromosome condensation and lagging chromosomes, which lead to impaired mitotic progression (4). We therefore decided to see whether altered chromatin structure could explain mitosis lengthening in *Omcg1*-deficient embryos. Immunofluorescence analyses were performed on E4.5 intercrosses embryos using antibodies directed against acetylated K9 of histone H3 and penta-acetylated histone H4. Methylation of histones was also analyzed using antibodies directed against trimethyl K27, dimethylated K4, and dimethylated K9 of histone H3. No dif-

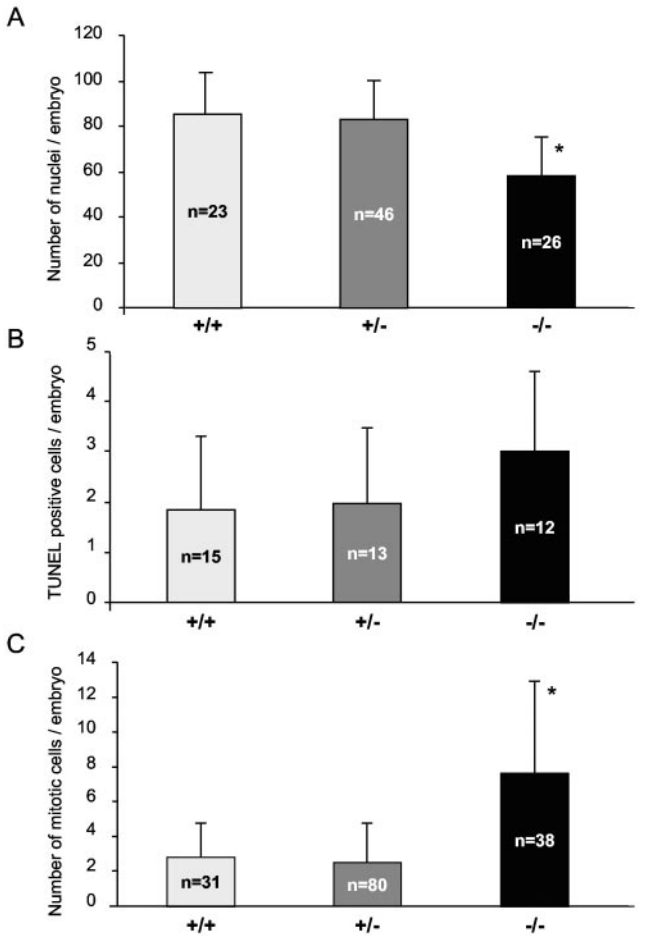

FIG. 7. Cell parameters of E4.5 *Omcg1*$^{+/-}$ intercross embryos. (A) Nuclei from E4.5 intercross blastocysts were stained with DAPI and counted under a fluorescent microscope. (B) TUNEL assay was performed to detect apoptotic cells in E4.5 embryos. (C) Determination of mitotic cell numbers was done by immunofluorescence with an anti-HH3ser10P antibody. In each experiment, embryos were recovered after microscopic examination and genotyped by nested PCR. Statistical analyses were performed by ANOVA. An asterisk indicates significant difference. *n*, number of embryos analyzed in each genotype.

ference between null and wild-type embryos was observed (unpublished data), suggesting that mitosis lengthening in *Omcg1*-deficient embryos is not associated with abnormal modifications of histones.

DISCUSSION

In the course of a search for candidate genes for an early lethal conditional mutation carried by the DDK mouse inbred strain, we identified a new gene, *Omcg1*, which codes for a nuclear 40-kDa protein, bearing a single zinc finger and two coiled-coil domains. This gene is evolutionarily conserved, and its function was yet unknown. To address its biological function, we disrupted the *Omcg1* locus via homologous recombination in ES cells. We found that *Omcg1*-deficient embryos die early in development, around the time of implantation, indicating that OMCG1 protein is essential for the completion of preimplantation development. Furthermore we could show that death of *Omcg1*$^{-/-}$ embryos coincides with or closely follows the depletion of the maternally derived OMCG1 protein, suggesting that the normal development of *Omcg1*$^{-/-}$ embryos until the blastocyst stage is due to the presence of maternally derived OMCG1 protein. We cannot, however, formally exclude a specific role of OMCG1 at the time of implantation.

The phenotype of *Omcg1*-null embryos is very severe and develops over a short period of time. Indeed, apparently normal *Omcg1*$^{-/-}$ blastocysts could be recovered from heterozygous intercrosses at E3.5; not only did they have an appearance indistinguishable from *Omcg1*$^{+/+}$ or *Omcg1*$^{+/-}$ embryos, but they also exhibited normal distribution of OCT-3/4 and TROMA-1 markers, indicating normal differentiation of the first two embryonic lineages, the TE and the ICM. However, when E3.5 intercross embryos were put in culture, the development of *Omcg1*$^{-/-}$ embryos appeared rapidly compromised: by 24 h, many of them exhibited morphological anomalies, and then the majority could not hatch, and all of them degenerated after 2 to 3 days in culture. Upon removal of their zona pellucida at E3.5, one-half of them attached to the dish, and some TE cells spread before degeneration. Thus, both TE and ICM development is compromised by *Omcg1* deficiency. In keeping with this observation, we were unable to produce homozygous null ES cells.

The finding that the mitotic index was affected and that chromosome segregation anomalies were observed in *Omcg1*$^{-/-}$ embryos before they died indicates that this gene is a key regulator of cell cycle progression. The diminution in cell number in E4.5 *Omcg1*$^{-/-}$ embryos was not due to an abnormal rate of apoptosis and was concomitant with an increase in the number of mitotic cells. This higher mitotic index did not correspond to an inability of the mutated embryonic cells to exit mitosis, as evidenced by the dramatic reduction of the number of mitotic cells in the *Omcg1*$^{-/-}$ embryos treated with mitomycin C, an agent that induces the DNA damage checkpoint. Absence of a mitotic block in *Omcg1*$^{-/-}$ embryos was also suggested by the nonaccumulation of mitotic cells in E4.5 *Omcg1*$^{-/-}$ embryos cultured for several hours, although *Omcg1*$^{-/-}$ cells were actively cycling as shown by BrdU incorporation. Thus, the mutated embryos, which have a lower number of cells, exhibit a higher mitotic index and at the same time retain the ability to exit mitosis. Altogether, these properties are best explained by a lengthening of the M phase.

One striking feature of *Omcg1* disruption is that both ICM and TE are affected. This is a situation which differs from the one observed for most knockouts of genes involved in the control of M phase (see, for example, references 6, 18, 30, and 46). Indeed, in these cases, blastocyst outgrowths of homozygous null embryos generally give rise to fairly normal differentiation of trophectoderm into giant cells. As giant cells undergo endoreplication cycles (alternative G and S phases), this might explain why these cells survive in the absence of genes specifically required during mitosis. The severe phenotype of the *Omcg1*$^{-/-}$ embryos indicates that *Omcg1* is functionally nonredundant and that a critical requirement for OMCG1 might take place before the differentiation into giant cells.

Interestingly, the lengthening of the cell cycle elicited by *Omcg1*-null embryos seems to be unique among the genes

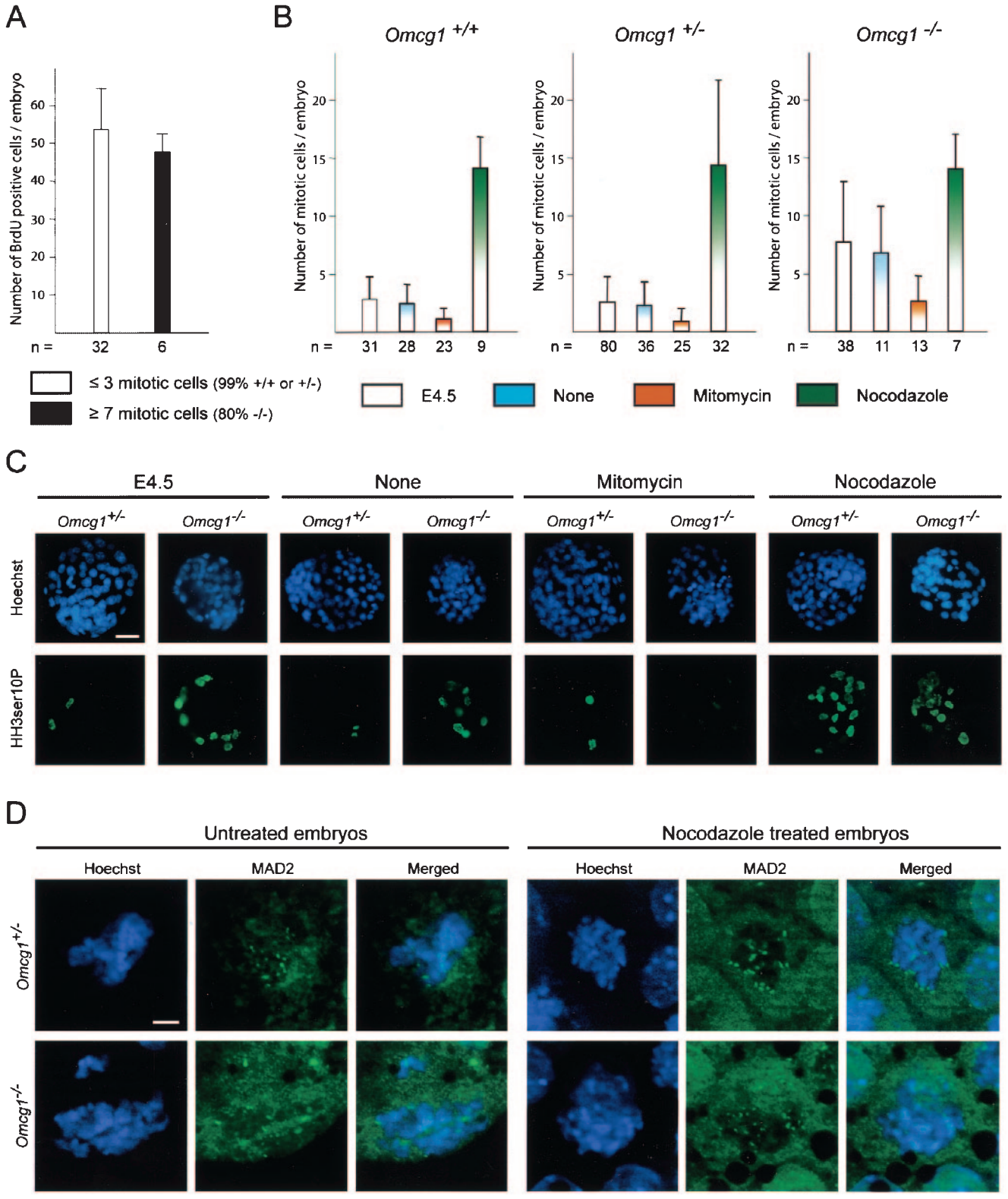

FIG. 8. Analysis of the cell cycle of E4.5 *Omcg1*$^{+/-}$ intercross embryos. (A) E4.5 intercross blastocysts were cultured for 3 h in the presence of BrdU. The number of BrdU-positive cells was counted using an anti-BrdU antibody in embryos with three or fewer mitotic cells (white box) and with seven or more mitotic cells (black box). (B) The number of mitotic cells was established, using an anti-HH3ser10P antibody, in E4.5 embryos from *Omcg1*$^{+/-}$ intercrosses cultured for different times and under different conditions: E4.5 embryos (white boxes), E4.5 embryos cultured for 7 h in absence of drugs (blue boxes), E4.5 embryos cultured for 7 h in the presence of mitomycin C (orange boxes), and E4.5 embryos cultured for 3 h in the presence of nocodazole (green boxes). *n*, number of embryos analyzed. (C) HH3ser10P immunofluorescence of embryos analyzed in panel B. Bar, 40 μm. (D) MAD2 immunofluorescence on mitotic cells from E4.5 intercross blastocysts with or without nocodazole treatment. Bar, 4 μm.

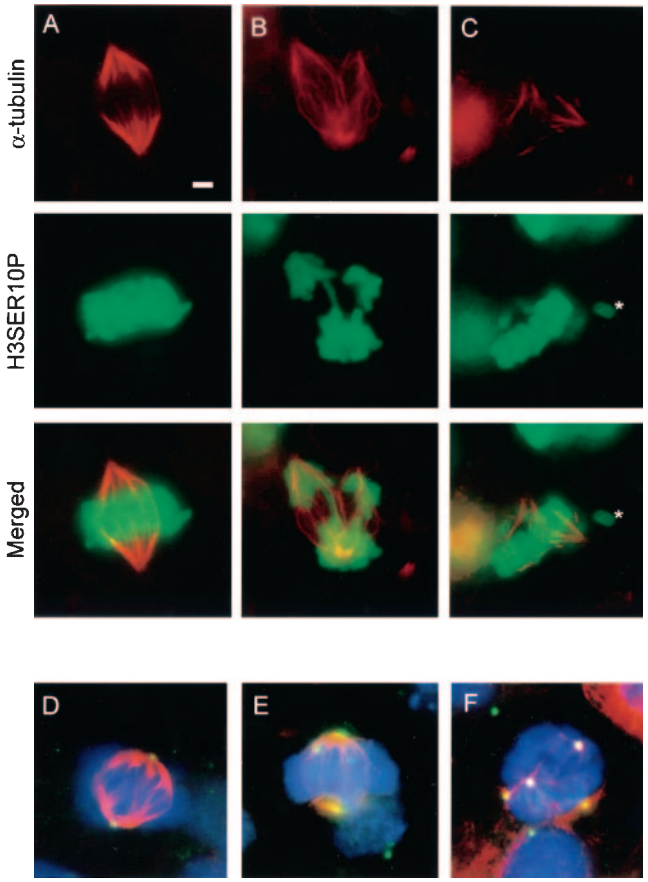

FIG. 9. Mitotic spindle defects in deficient embryos. E4.5 *Omcg1*$^{-/-}$ blastocysts were stained with Hoechst 33342 (blue), anti-α-tubulin (red), and anti-HH3ser10P or anti-γ-tubulin antibodies (green). (A) Normal organization of the spindle and the metaphasic plate in an *Omcg1*$^{-/-}$ cell. Some *Omcg1*$^{-/-}$ cells displayed abnormal spindles, for example, a tripolar spindle (B) or misalignment between spindle and chromosomes accompanied by isolated chromosomes (C, asterisk). (D) Normal organization of the mitotic spindle was often associated with two centrosomes. (E and F) Some *Omcg1*-null cells exhibited abnormal numbers of centrosomes. In nonmitotic cells, centrosomes were stained green, while in mitotic cells they were stained yellow because of the colocalization of α- and γ-tubulin to the poles of the spindle. Bar, 2 μm.

functionally implicated in the preimplantation development. Indeed, while a high mitotic index at the end of preimplantation development was reported for a few knock-out mice, it generally resulted from a mitotic block (25, 28, 32). For example, late blastocysts homozygous for the mutation oligosyndactyly, a radiation-induced mutation causing the disruption of the anaphase-promoting complex component APC10/DOC1 (41), have an elevated mitotic index due to a cell-autonomous block in the transition from metaphase to anaphase (32). Similarly, in the absence of *E4F*, a gene encoding a transcription factor, cells of E4.5 blastocysts fail to progress through the M phase and accumulate at the prometaphase (25). How *Omcg1* deficiency leads to a mitotic delay is not yet known. Nevertheless, we frequently observed abnormal mitotic figures including disorganized mitotic spindle, abnormal number of centrosomes, and misaligned chromosomes in *Omcg1*$^{-/-}$ embryos. In addition, our observation of plurinucleated cells in *Omcg1*$^{-/-}$ cultured blastocysts suggests that *Omcg1*$^{-/-}$ cells eventually exited mitosis without undergoing cytokinesis. All general delays in mitosis are mediated by the spindle assembly checkpoint, and many conditions such as DNA damage or histone deacetylation can prevent the satisfaction of this checkpoint (for a review, see reference 42). *Omcg1*-deficient embryos are provided with a functional spindle checkpoint as demonstrated by mitotic index increase and MAD2 recruitment on kinetochores upon nocodazole treatment. Lengthening of mitosis in these embryos does not seem to be due to DNA damage as it would imply that the G_2 DNA damage checkpoint is defective, a situation which is not supported by the observed blockade of *Omcg1*-null embryos upon mitomycin C treatment. Overall, histone acetylation and methylation analysis indicates that it does not seem to be due to abnormal chromatin remodeling.

It should be noted that although *Omcg1* is evolutionarily conserved, it may not be an essential gene in all species or in all tissues. Indeed, RNA interference-mediated knock-down of T04A8.10, the *C. elegans Omcg1* gene, does not lead to defects in cell division as monitored by differential interference contrast examination of early embryos (15). Similarly, a genome-wide RNA interference screen for genes involved in growth and viability of embryonic hemocyte cell lines did not pick up CG11839, the *Drosophila melanogaster Omcg1* gene (3). Taken together, these data suggest that, in these organisms, *Omcg1* is dispensable for basic cellular processes such as cell division. It is possible, however, that *Omcg1* acquired a new and essential function during evolution, maybe through the acquisition of a central domain which is lacking in the worm and fly proteins but present in the mouse protein.

In summary, we have characterized a new gene and demonstrated that it plays an essential role in preimplantation development by controlling different aspects of the M phase. Absence of OMCG1 precluded the development of both TE and ICM. Early embryonic death of *Omcg1*$^{-/-}$ embryos and the failure to establish a homozygous null ES cell line have prevented us from defining more precisely its role in the control of the M phase in early embryonic cells. Future work, including the use of conditional gene targeting, should allow us to decipher the molecular mechanisms underlying its biological action.

ACKNOWLEDGMENTS

We thank Tiphaine Aguirre-Lavin for technical assistance; Katja Wassmann for helpful suggestions in the analysis of the spindle checkpoint; Julie Chaumeil and Edith Heard for their advice in the analysis of histone modifications; Sarah Cormier and Céline Souilhol for helpful discussion; and Michel Bornens, Shahragim Tajbakhsh, and Marie-Hélène Verlhac for critical reading of the manuscript. We are also very grateful to Pascal Roux and Emmanuelle Perret, Plateforme d'Imagerie Dynamique, Institut Pasteur, for technical assistance.

This work was supported by the Centre National de la Recherche Scientifique, the Institut Pasteur GPH07 on stem cells, and the "Action concertée incitative Biologie du Développement et Physiologie Intégrative" from the Ministère de l'Education Nationale, de la Recherche et de la Technologie. J.A. received funding from the Ministère de l'Education Nationale, de la Recherche et de la Technologie.

REFERENCES

1. **Babinet, C., V. Richoux, J. L. Guenet, and J. P. Renard.** 1990. The DDK inbred strain as a model for the study of interactions between parental genomes and egg cytoplasm in mouse preimplantation development. Dev. Suppl. **1990:**81–87.

2. **Berthet, C., E. Aleem, V. Coppola, L. Tessarollo, and P. Kaldis.** 2003. Cdk2 knockout mice are viable. Curr. Biol. **13:**1775–1785.
3. **Boutros, M., A. A. Kiger, S. Armknecht, K. Kerr, M. Hild, B. Koch, S. A. Haas, H. F. Consortium, R. Paro, and N. Perrimon.** 2004. Genome-wide RNAi analysis of growth and viability in *Drosophila* cells. Science **303:**832–835.
4. **Cimini, D., M. Mattiuzzo, L. Torosantucci, and F. Degrassi.** 2003. Histone hyperacetylation in mitosis prevents sister chromatid separation and produces chromosome segregation defects. Mol. Biol. Cell **14:**3821–3833.
5. **Cohen-Tannoudji, M., S. Vandormael-Pournin, S. Le Bras, F. Coumailleau, C. Babinet, and P. Baldacci.** 2000. A 2-Mb YAC/BAC-based physical map of the ovum mutant (Om) locus region on mouse chromosome 11. Genomics **68:**273–282.
6. **Dobles, M., V. Liberal, M. L. Scott, R. Benezra, and P. K. Sorger.** 2000. Chromosome missegregation and apoptosis in mice lacking the mitotic checkpoint protein Mad2. Cell **101:**635–645.
7. **Edgar, B. A., and C. F. Lehner.** 1996. Developmental control of cell cycle regulators: a fly's perspective. Science **274:**1646–1652.
8. **Elledge, S. J.** 1996. Cell cycle checkpoints: preventing an identity crisis. Science **274:**1664–1672.
9. **Fay, D. S., and M. Han.** 2000. Mutations in *cye-1*, a *Caenorhabditis elegans* cyclin E homolog, reveal coordination between cell-cycle control and vulval development. Development **127:**4049–4060.
10. **Fischle, W., Y. Wang, and C. D. Allis.** 2003. Histone and chromatin cross-talk. Curr. Opin. Cell Biol. **15:**172–183.
11. **Flach, G., M. H. Johnson, P. R. Braude, R. A. Taylor, and V. N. Bolton.** 1982. The transition from maternal to embryonic control in the 2-cell mouse embryo. EMBO J. **1:**681–686.
12. **Friedrich, G., and P. Soriano.** 1991. Promoter traps in embryonic stem cells: a genetic screen to identify and mutate developmental genes in mice. Genes Dev. **5:**1513–1523.
13. **Fulka, J., Jr., N. L. First, J. Fulka, and R. M. Moor.** 1999. Checkpoint control of the G2/M phase transition during the first mitotic cycle in mammalian eggs. Hum. Reprod. **14:**1582–1587.
14. **Geng, Y., Q. Yu, E. Sicinska, M. Das, J. E. Schneider, S. Bhattacharya, W. M. Rideout, R. T. Bronson, H. Gardner, and P. Sicinski.** 2003. Cyclin E ablation in the mouse. Cell **114:**431–443.
15. **Gonczy, P., C. Echeverri, K. Oegema, A. Coulson, S. J. Jones, R. R. Copley, J. Duperon, J. Oegema, M. Brehm, E. Cassin, E. Hannak, M. Kirkham, S. Pichler, K. Flohrs, A. Goessen, S. Leidel, A. M. Alleaume, C. Martin, N. Ozlu, P. Bork, and A. A. Hyman.** 2000. Functional genomic analysis of cell division in *C. elegans* using RNAi of genes on chromosome III. Nature **408:**331–336.
16. **Harlow, G. M., and P. Quinn.** 1982. Development of preimplantation mouse embryos in vivo and in vitro. Aust. J. Biol. Sci. **35:**187–193.
17. **Hendzel, M. J., Y. Wei, M. A. Mancini, A. Van Hooser, T. Ranalli, B. R. Brinkley, D. P. Bazett-Jones, and C. D. Allis.** 1997. Mitosis-specific phosphorylation of histone H3 initiates primarily within pericentromeric heterochromatin during G2 and spreads in an ordered fashion coincident with mitotic chromosome condensation. Chromosoma **106:**348–360.
18. **Kalitsis, P., E. Earle, K. J. Fowler, and K. H. Choo.** 2000. Bub3 gene disruption in mice reveals essential mitotic spindle checkpoint function during early embryogenesis. Genes Dev. **14:**2277–2282.
19. **Kang, S. G., H. Chung, Y. D. Yoo, J. G. Lee, Y. I. Choi, and Y. S. Yu.** 2001. Mechanism of growth inhibitory effect of mitomycin-C on cultured human retinal pigment epithelial cells: Apoptosis and cell cycle arrest. Curr. Eye Res. **22:**174–181.
20. **Knoblich, J. A., K. Sauer, L. Jones, H. Richardson, R. Saint, and C. F. Lehner.** 1994. Cyclin E controls S phase progression and its down-regulation during *Drosophila* embryogenesis is required for the arrest of cell proliferation. Cell **77:**107–120.
21. **Kozar, K., M. A. Ciemerych, V. I. Rebel, H. Shigematsu, A. Zagozdzon, E. Sicinska, Y. Geng, Q. Yu, S. Bhattacharya, R. T. Bronson, K. Akashi, and P. Sicinski.** 2004. Mouse development and cell proliferation in the absence of D-cyclins. Cell **118:**477–491.
22. **Kress, C., S. Vandormael-Pournin, P. Baldacci, M. Cohen-Tannoudji, and C. Babinet.** 1998. Nonpermissiveness for mouse embryonic stem (ES) cell derivation circumvented by a single backcross to 129/Sv strain: establishment of ES cell lines bearing the Omd conditional lethal mutation. Mamm. Genome **9:**998–1001.
23. **Kruhlak, M. J., M. J. Hendzel, W. Fischle, N. R. Bertos, S. Hameed, X. J. Yang, E. Verdin, and D. P. Bazett-Jones.** 2001. Regulation of global acetylation in mitosis through loss of histone acetyltransferases and deacetylases from chromatin. J. Biol. Chem. **276:**38307–38319.
24. **Le Bras, S., M. Cohen-Tannoudji, V. Guyot, S. Vandormael-Pournin, F. Coumailleau, C. Babinet, and P. Baldacci.** 2002. Transcript map of the *Ovum mutant* (*Om*) locus: isolation by exon trapping of new candidates genes for the DDK syndrome. Gene **296:**75–86.
25. **Le Cam, L., M. Lacroix, M. A. Ciemerych, C. Sardet, and P. Sicinski.** 2004. The E4F protein is required for mitotic progression during embryonic cell cycles. Mol. Cell. Biol. **24:**6467–6475.
26. **Levine, E. M.** 2004. Cell cycling through development. Development **131:**2241–2246.
27. **Li, R., and A. W. Murray.** 1991. Feedback control of mitosis in budding yeast. Cell **66:**519–531.
28. **Li, T., A. Inoue, J. M. Lahti, and V. J. Kidd.** 2004. Failure to proliferate and mitotic arrest of CDK11$^{p110/p58}$-null mutant mice at the blastocyst stage of embryonic cell development. Mol. Cell. Biol. **24:**3188–3197.
29. **Li, Y., and R. Benezra.** 1996. Identification of a human mitotic checkpoint gene: hsMAD2. Science **274:**246–248.
30. **Liu, Q., S. Guntuku, X. S. Cui, S. Matsuoka, D. Cortez, K. Tamai, G. Luo, S. Carattini-Rivera, F. DeMayo, A. Bradley, L. A. Donehower, and S. J. Elledge.** 2000. Chk1 is an essential kinase that is regulated by Atr and required for the G(2)/M DNA damage checkpoint. Genes Dev. **14:**1448–1459.
31. **Mac Auley, A., Z. Werb, and P. E. Mirkes.** 1993. Characterization of the unusually rapid cell cycles during rat gastrulation. Development **117:**873–883.
32. **Magnuson, T., and C. J. Epstein.** 1984. Oligosyndactyly: a lethal mutation in the mouse that results in mitotic arrest very early in development. Cell **38:**823–833.
33. **Malumbres, M., R. Sotillo, D. Santamaria, J. Galan, A. Cerezo, S. Ortega, P. Dubus, and M. Barbacid.** 2004. Mammalian cells cycle without the D-type cyclin-dependent kinases Cdk4 and Cdk6. Cell **118:**493–504.
34. **Mortensen, R. M., D. A. Conner, S. Chao, A. A. Geisterfer-Lowrance, and J. G. Seidman.** 1992. Production of homozygous mutant ES cells with a single targeting construct. Mol. Cell. Biol. **12:**2391–2395.
35. **Newport, J., and M. Kirschner.** 1982. A major developmental transition in early *Xenopus* embryos. I. Characterization and timing of cellular changes at the midblastula stage. Cell **30:**675–686.
36. **O'Farrell, P. H., J. Stumpff, and T. T. Su.** 2004. Embryonic cleavage cycles: how is a mouse like a fly? Curr. Biol. **14:**R35–45.
37. **Ortega, S., I. Prieto, J. Odajima, A. Martin, P. Dubus, R. Sotillo, J. L. Barbero, M. Malumbres, and M. Barbacid.** 2003. Cyclin-dependent kinase 2 is essential for meiosis but not for mitotic cell division in mice. Nat. Genet. **35:**25–31.
38. **Pagano, M., and P. K. Jackson.** 2004. Wagging the dogma: tissue-specific cell cycle control in the mouse embryo. Cell **118:**535–538.
39. **Pardee, A. B.** 1989. G1 events and regulation of cell proliferation. Science **246:**603–608.
40. **Parisi, T., A. R. Beck, N. Rougier, T. McNeil, L. Lucian, Z. Werb, and B. Amati.** 2003. Cyclins E1 and E2 are required for endoreplication in placental trophoblast giant cells. EMBO J. **22:**4794–4803.
41. **Pravtcheva, D. D., and T. L. Wise.** 2001. Disruption of Apc10/Doc1 in three alleles of oligosyndactylism. Genomics **72:**78–87.
42. **Rieder, C. L., and H. Maiato.** 2004. Stuck in division or passing through: what happens when cells cannot satisfy the spindle assembly checkpoint. Dev. Cell **7:**637–651.
43. **Rieder, C. L., A. Schultz, R. Cole, and G. Sluder.** 1994. Anaphase onset in vertebrate somatic cells is controlled by a checkpoint that monitors sister kinetochore attachment to the spindle. J. Cell Biol. **127:**1301–1310.
44. **Robertson, E. J., and A. Bradley.** 1986. Production of permanent cell lines from early embryos and their use in studying developmental problems, p. 475–508. *In* J. R. R. A. Pedersen (ed.), Experimental approaches to mammalian embryonic development. IRL Press, Oxford, United Kingdom.
45. **Snow, M. H. L.** 1977. Gastrulation in mouse: growth and regionalization of epiblast. J. Embryol. Exp. Morphol. **42:**293–303.
46. **Takai, H., K. Tominaga, N. Motoyama, Y. A. Minamishima, H. Nagahama, T. Tsukiyama, K. Ikeda, K. Nakayama, and M. Nakanishi.** 2000. Aberrant cell cycle checkpoint function and early embryonic death in Chk1$^{-/-}$ mice. Genes. Dev. **14:**1439–1447.
47. **Thompson, J. D., D. G. Higgins, and T. J. Gibson.** 1994. CLUSTAL W: improving the sensitivity of progressive multiple sequence alignment through sequence weighting, position-specific gap penalties and weight matrix choice. Nucleic Acids Res. **22:**4673–4680.
48. **Varmuza, S., V. Prideaux, R. Kothary, and J. Rossant.** 1988. Polytene chromosomes in mouse trophoblast giant cells. Development **102:**127–134.
49. **Wassmann, K., T. Niault, and B. Maro.** 2003. Metaphase I arrest upon activation of the Mad2-dependent spindle checkpoint in mouse oocytes. Curr. Biol. **13:**1596–1608.
50. **Whittingham, D. G., and R. G. Wales.** 1969. Storage of two-cell mouse embryos in vitro. Aust. J. Biol. Sci. **22:**1065–1068.
51. **Yagi, T., Y. Ikawa, K. Yoshida, Y. Shigetani, N. Takeda, I. Mabuchi, T. Yamamoto, and S. Aizawa.** 1990. Homologous recombination at *c-fyn* locus of mouse embryonic stem cells with use of diphtheria toxin A-fragment gene in negative selection. Proc. Natl. Acad. Sci. USA **87:**9918–9922.